Vibrational properties of High Entropy Alloy based metal hydrides probed by inelastic neutron scattering

Gustav Ek [a],[*], Øystein S. Fjellvåg [b], Ponniah Vajeeston [c], Jeff Armstrong [d], Martin Sahlberg [a], Ulrich Häussermann [e]

[a] Department of Chemistry – Ångström Laboratory, Uppsala University, Box 523, SE-75120 Uppsala, Sweden
[b] Institute for Energy Technology, Department of Neutron Materials Characterization, P.O Box 40, NO-2027, Kjeller, Norway
[c] Centre for Materials Science and Nanotechnology, Department of Chemistry, University of Oslo, P.O Box 1033, NO-0315 Oslo, Norway
[d] ISIS Pulsed Neutron and Muon source, Rutherford Appleton Laboratory, OX11 0QX Didcot, United Kingdom
[e] Department of Materials and Environmental Chemistry, Stockholm University, SE-10691 Stockholm, Sweden

ARTICLE INFO

ABSTRACT

The vibrational properties of several High Entropy Alloy (HEA) based metal hydrides are investigated by inelastic neutron scattering (INS). HEAs have recently emerged as a new type of materials with a wide range of intriguing properties and potential applications such as hydrogen storage. The special properties of HEAs are believed to originate from the disordered lattice and internal strain that is introduced from the differences in atomic radii. This makes HEA hydrides provide an intriguing situation for the local H coordination, of several different transition metals. INS spectra were collected on a series of HEA-based metal hydrides starting with TiVNbH$_x$ and subsequently adding Zr and Hf to increase the atomic size mismatch. A general feature of the spectra are the optical peaks centered around an energy loss of 150 meV that can be attributed to hydrogen vibrations in a tetrahedral environment. Upon the addition of Zr and Hf, a shoulder appears on the optical peak at lower energy transfers that after comparison with *in silico* calculated INS spectra is indicative of hydrogen also occupying octahedral sites in the structure.

1. Introduction

High entropy alloys (HEA) have recently emerged as a new type of materials with a wide range of intriguing properties and potential applications. A HEA is built on an equimolar mix of several different metals (typically five or more) with different sizes and is stabilised by the high entropy of mixing [1]. The average structure of a HEA typically corresponds to one of the simple crystal structures such as body-centred cubic (bcc) and cubic close packed (ccp). The special properties of HEAs are believed to originate from the disordered lattice and internal strain that is introduced from e.g. the differences in atomic radii and the valence electron concentration [2]. As with many intermetallic compounds, HEAs are capable of absorbing large quantities of hydrogen [3–12]. Remarkably, it has been shown that HEAs exclusively based on transition metals can accommodate hydrogen in both tetrahedral and octahedral interstitial sites [5,8]. Thus, the hydrogen storage capacity of transition metals, which is

typically limited to H/M ≤ 2, may be exceeded with HEAs. In addition, HEA hydrides provide an interesting situation for the local H coordination, which constitutes several different transition metals. The salient questions are the dependence of H content and distribution of H atoms on the chemical composition of the HEA, as well as potential changes in the local structure of the HEAs introduced by the incorporated H.

A good indication of site preference in the typical metal lattices has been suggested by *Hauck,* by comparing the electronegativity of the host metal atom to that of hydrogen [13]. Suppose the hydrogen is less electronegative than the host metal. In that case, it will tend to lose its electron to the metal conduction band, and therefore prefer the interstitial site with the highest electron density, which is the octahedral site. If, on the other hand it is more electronegative, it will prefer the smaller tetrahedral site. This effect is clearly visible in the V-H/D system, where V has electronegativity close to that of hydrogen, and random occupation of both octahedral and tetrahedral interstitials [14]. Less electronegative metals also tend to have larger unit cell parameters.

Inelastic Neutron Scattering (INS) provides accurate information about the vibrations of hydrogen due to its large incoherent

* Corresponding author.
  E-mail address: gustav.ek@kemi.uu.se (G. Ek).

scattering cross section compared to the host metal lattice. Furthermore, since the hydrogen essentially exists as H$^-$ in the CaF_2 type hydrides, the fundamental hydrogen vibrations can be well correlated with the unit cell parameters or M-H distances [15,16]. From earlier works on transition and rare-earth metal hydrides, it has been shown that the vibrations of hydrogen occupying the octahedral tetrahedral and interstitials are well separated in the energy loss ranges of 40 < −70 meV and 100–140 meV respectively [17–19]. Shapes and splits of bands can give information about the chemical environment, the degree of local disorder, or H-H interactions [20,21].

In this work, the vibrational properties of hydrogen have been studied using INS in a series of HEA-based metal hydrides starting with the quaternary TiVNbH$_x$ and subsequently adding Zr and Hf to increase the chemical disorder in the system. In addition, TiZrHf was also chosen due to its ability to form a metal hydride with body-centered tetragonal (bct) lattice.

2. Experimental

The alloys were produced by arc-melting stoichiometric amounts of the constituent elements Ti (Goodfellow, 99.99% metals basis), V (Goodfellow, 99.6% metal basis), Nb (Goodfellow, 99.9% metals basis), Zr (Goodfellow, 99.2% metals basis, max 0.8% Hf) and Hf (ChemPur, 99.8% metals basis excluding Zr) under Ar atmosphere. Prior to melting the chamber was purified by melting a Ti-getter piece to reduce O$_2$ contamination in the chamber. Samples were remelted five times and flipped between each melting to improve their chemical homogeneity. The ingots (sample sizes ~15 g) were then cut into smaller pieces before hydrogenation. Hydrides were synthesized by solid-gas reaction in a home-built Sieverts type apparatus [22]. The alloys were activated by heating to 340 °C for 2 h under dynamic vacuum, followed by cooling down to room temperature. Samples were then subjected to hydrogen gas of pressures around 60 bar in a single pulse and left under these conditions until the pressure difference was below the detection limits of the pressure transducer ±0.3 bar. The only exception to this procedure is TiZrHf which has very slow hydrogen sorption kinetics at room temperature, and requires activation at 500 °C for 2 h followed by hydrogen exposure at 300 °C. After hydrogenation the samples were ground into a fine powder using an agate mortar. All sample handling was conducted in an Ar filled glovebox with O$_2$ and H$_2$O levels <1 ppm.

Powder X-ray diffraction was conducted on a Bruker D8 Advance diffractometer using Cu K$_\alpha$ radiation in capillary mode. Structural parameters were determined by the Rietveld method implemented in the software Topas Academic [23,24].

Inelastic neutron spectra were collected at the TOSCA instrument at the ISIS Neutron and Muon spallation source in the United Kingdom. Hydride powders (10 g per sample) were packed in flat Al cans with a cross-sectional area of 4.0 × 4.8 cm^2 and spectra were collected at the base temperature of the instrument (~20 K) [25,26].

Total energies were calculated by the projected-augmented planewave (PAW) implementation of the Vienna ab initio simulation package (VASP) [27,28]. Two set of calculations were made, one with local density approximation (LDA) and another with the Perdew, Burke, and Ernzerhof (PBE) [29] exchange correlation functional with the Hubbard parameter correction (LDA+U), following the rotationally invariant form [30,31]. Effective U values of 4.4 eV, 2.7 eV, and 2.1 eV were used for the Ti-d, V-d and Nb-d states, respectively, and the effective on-site exchange interaction parameter J was fixed to 1 eV.

Ground-state geometries of the mono and di-hydrides (MH, MH_2; where M = Ti, V, Zr, Nb, and Hf) were determined by minimizing stresses and Hellman-Feynman forces using the conjugate-gradient algorithm with force convergence less than 10^{-3} eV Å^{-1}. Brillouin

zone integrations were performed with a Gaussian broadening of 0.1 eV during all relaxations. From various sets of calculations it was found that 512 k-points in the whole Brillouin zone for the structure with a 600 eV plane-wave cutoff are sufficient to ensure optimum accuracy in the computed results. The k-points were generated using the Monkhorst-Pack method with a grid size of 8 × 8 × 8 for structural optimization. A similar density of k-points and energy cutoff was used to estimate total energy as a function of volume for all the structures considered in the present work.

A frozen phonon calculation was applied to the supercells using the Phonopy program to obtain the phonon dispersion curve and phonon density of states [32]. An atomic displacement of 0.01 Å was used for symmetry consideration to obtain the force constants for the phonon calculations. The displacements in opposite directions along all possible axes were incorporated in the calculations to improve the precision. The force calculations were made using the VASP code with the supercell approach (with LDA+U correction) and the resulting data were imported into the Phonopy program. The dynamical matrices were calculated from the force constants, and phonon density of states (PhDOS) curves was computed using the Monkhorst-Pack scheme [33]. Phonon calculations were weighed with the neutron cross sections [34] of the elements (Ti, V, Zr, Nb, Hf) using the AbINS plugin in the Mantid software to obtain the *in silico* INS spectra [35,36].

3. Results and discussion

The investigated HEAs (Fig. 1) alloys crystallize in a bcc (W-type, *Im-3 m*) structure except for TiZrHf which adopts a hcp (*P6$_3$/mmc*) arrangement with unit cell parameters presented in Table 1. After hydrogen exposure, all hydrides can be indexed as either fcc (*Fm$\bar{3}$m*) or bct (*I4/mmm*) which is indicative of CaF_2-type structures common for metal hydrides with hydrogen per metal ratios close to
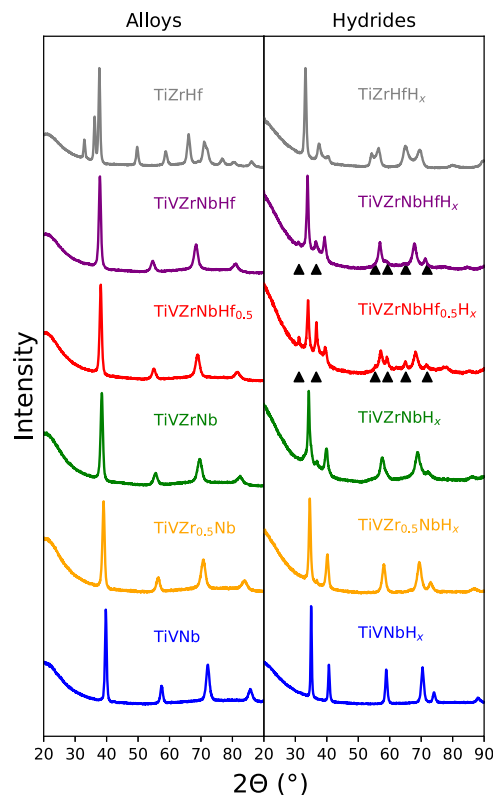

Fig. 1. Powder X-Ray diffraction patterns of the HEAs (left) and their corresponding metal hydrides (right). Contributions from C14-type Laves phases are marked by triangles.

Table 1

Summary of the unit cell parameters, hydrogen contents, Pauling electronegativity (χ_p), valence electron concentration (VEC) and atomic size mismatch (δ) of the investigated bcc HEAs and their corresponding hydrides.

Alloy	$a_{bcc/hex}$ (Å)	c_{hex} (Å)	$a_{fcc/bct}$ (Å)	c_{bct} (Å)	H content (wt%)	χ_p (Ø)	VEC (Ø)	δ (%)
TiVNb	3.2034(1)	–	4.4353(8)	–	3.00	1.59	4.67	3.81
TiVZr$_{0.5}$Nb	3.2611(2)	–	4.4905(2)	–	2.87	1.55	4.57	5.43
TiVZrNb	3.3068(2)	–	4.5249(4)	–	2.77	1.53	4.50	6.03
TiVZrNbHf$_{0.5}$	3.3343(2)	–	4.5574(2)	–	2.28	1.50	4.44	6.10
TiVZrNbHf	3.5635(2)	–	4.5816(6)	–	2.09	1.48	4.40	6.08
TiZrHf	3.1377(2)	4.9591(3)	3.3766(5)	4.4856(1)	1.96	1.39	4.00	4.00

2 (1.9 in the investigated samples). This is supported by previous neutron diffraction studies which showed that TiVNb-based HEA metal deuterides adopts CaF$_2$-type structures with deuterium predominately situated in the tetrahedral interstitial positions (1/4,1/4,1/4) of the cubic structure [37–39]. Additionally, TiVZr$_{0.5}$NbH$_x$ and TiVZrNbH$_x$ show one small Bragg peak in between the two main fcc peaks. This feature is more evident when Hf is added. These additional Bragg peaks can be indexed as a C14-type Laves phase. The phase separation is most likely due to the heat generated during the exothermic hydrogenation reaction with a large sample size (15 g), as annealing experiments on TiVZrNbHf has shown the emergence of a similar Laves phase at temperatures above 600 °C [40]. The Laves phase does not appear to absorb hydrogen under the conditions of this work and should therefore have a negligible impact on the INS spectra.

Fig. 2 shows the measured INS spectra for the investigated HEA-based metal hydrides. The spectra's main feature is the optical peaks centered around an energy loss of 150 meV that can be attributed to the fundamental vibration of tetrahedral interstitial hydrogen in a fcc lattice. The peaks at higher energy transfer are higher harmonics of the optical peak. The metal phonons are located below 20 meV in the spectra. Noticeably, the optical peak is split in the simplest system, TiVNbH$_x$. The split of the optical peak is similar to that found in the classical ZrH$_2$ [21] which was believed to be caused by the tetragonal distortion of the cubic symmetry, causing degeneracy between vibrations parallel or in-plane perpendicular to the c-axis. The split of the peaks was directly proportional to the c/a ratio in ZrH$_2$ of 1.12 resulting in a 12% peak separation. However, here we observe this feature for a cubic system.

Another noteworthy feature from the measured spectra is that the split starts to be less pronounced once Zr is added to the HEA-based metal hydrides. An additional change is present when adding Hf, where the intensity of the degenerate peaks are suppressed to almost the same magnitude. A shoulder also appears on the lower energy transfer side of the optical peaks (80–120 meV) upon the addition of Zr and Hf. A similar shoulder has been observed in ZrV$_2$H$_{4.5}$ and TiVH systems. The literature attributes the shoulder to an intermediate V$_4$ site between tetrahedral and octahedral energy loss [41,42]. Another possible explanation is that the shoulder
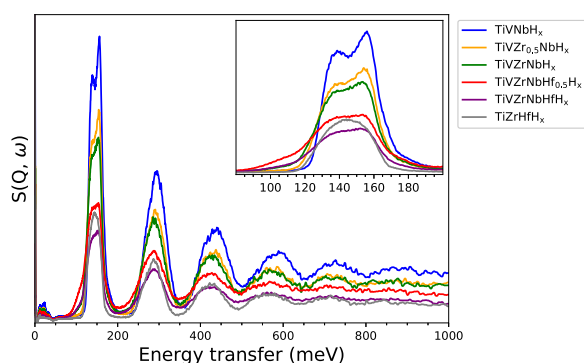
originates from an octahedral site. The rare-earth metal hydrides, where both tetrahedral and octahedral interstitials are filled, have shown to have the octahedral energy loss range in 60–80 meV [17–19] and transition based monohydrides in the range 60–120 meV [43].

In the crystal structure of a HEA, all the metal atoms occupy the same crystallographic site. Therefore, modelling their properties requires very large unit cells for a representative analysis and is therefore computationally expensive. With this in mind, we have calculated *in silico* INS spectra for the binary transition metal hydrides to approach the HEA, presented in Fig. 3. We first note that both the LDA and GGA functionals give similar shape to the vibrational density of states, and that LDA tends to underestimate the crystallographic volumes more than GGA (hence we will use GGA for further analysis). We also note that all the cubic CaF$_2$-type hydrides show a splitting of the optical peak, as we observed in our experimental INS of the HEAs, and is reported for the ZrV$_2$H$_{4.5}$ and TiVH systems [41,42]. Similar behavior has been found in calculations for ZrH$_2$ [44,45], where it was found that the splitting originates from different optical phonons and not structural distortions, which is in agreement with our calculations (the different phonons are presented as supplementary gifs). In fact, the phonon dispersion is quite complex, giving rise to several features in the vibrational density of states.

Comparing the experimental HEA-based metal hydrides with the *in silico* spectra (considering the shift towards higher energy transfers) it is evident that the HEAs' H vibrations are situated closely to that of their corresponding binary metal hydrides. TiVNbH$_x$ and TiZrHfH$_x$ is in good compliance with the *in silico* spectra of the constituent binary hydrides, which is foreseeable, as the alloys have very closely related characteristics to the elements in terms of size, electronegativity and valence electrons as seen in Table 1. Noteworthy, the sum of the calculated INS spectra show more detailed structures than the experimental ones. Considering the resolution of TOSCA is around 2% at this energy means that in this case, the less defined M-H bond lengths of the HEAs most likely hide these features from the spectra. This effect of broad peaks even at low temperatures has also been reported in the literature for similar compositions such as metal hydrides based on the elements Ti-V-Cr-Mo and more recently the HEA TiVCrNbH$_x$ [20,46] where it is indicative of local disorder.

The *in silico* spectra shown in Fig. 3 do not explain the shoulder to higher energy losses present in all the investigated HEA-based metal hydrides, nor the lower energy shoulder that appears once Zr and Hf is added. The higher energy shoulder can originate from two-phonon neutron scattering involving the optical phonon mode and the low energy acoustic modes, as similar features have been observed in the literature for metal hydrides such as ScH$_x$ [47]. Alternatively, these features have also been seen in metal hydrides based on elements in groups VI-VIII [43] where it was assumed that these belonged to longitudinal optical transverse modes stemming from long-range repulsive H-H interactions. To investigate the origin of the high-energy shoulder, we calculated the *in silico* INS spectra of the metal hydrides with two quantum events. In these spectra, we observe a shoulder that appears at higher energy transfers than the optical
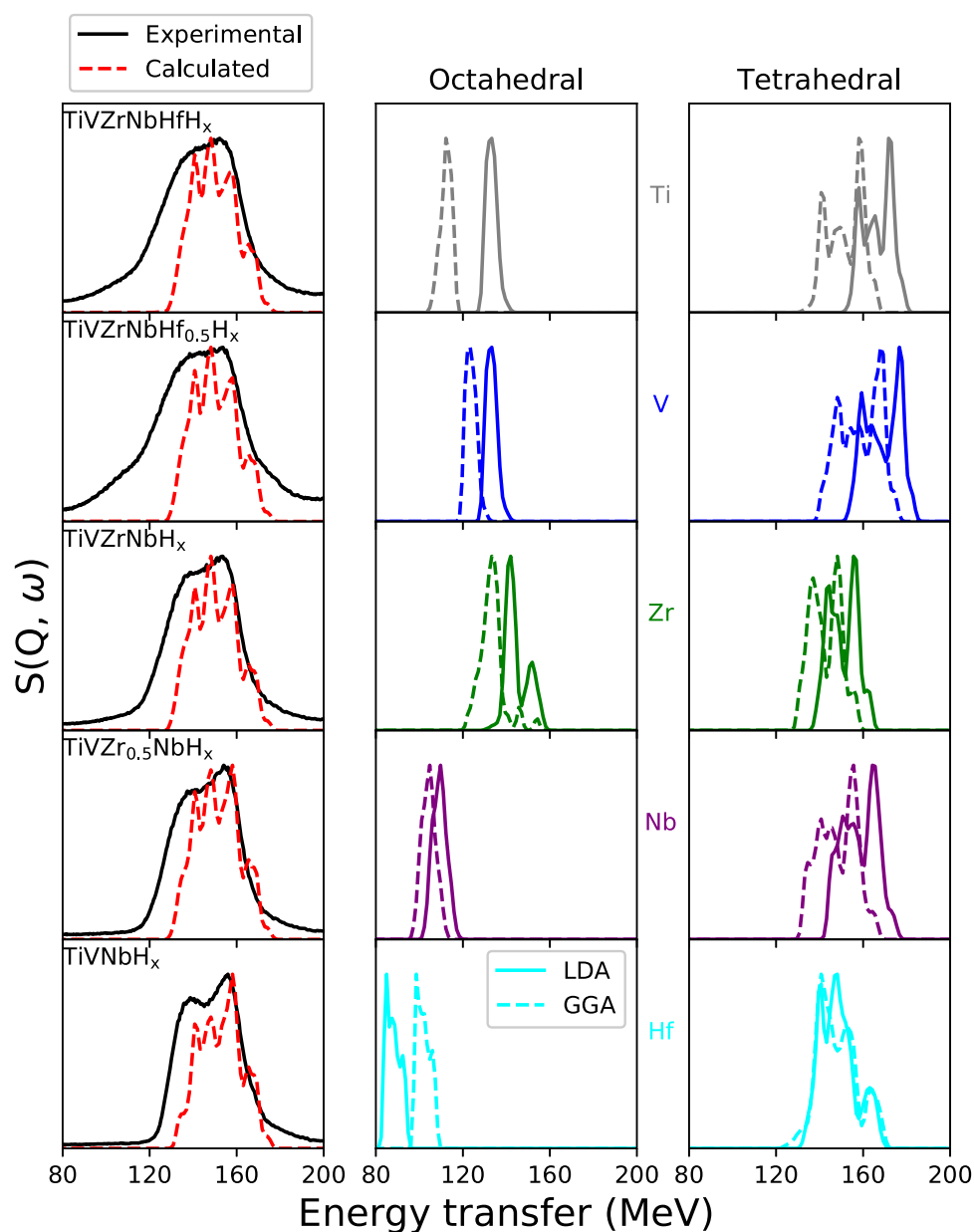

Fig. 2. Measured INS spectra of the HEA-based metal hydrides.

Fig. 3. Comparison of in silico calculated and experimental vibrational spectra where the calculated constitutes a combination of the binary MH_2 hydrides using GGA (left) and in silico INS spectra of binary metal hydrides for hydrogen occupation in both octahedral (middle) and tetrahedral interstitial sites (right). Measured HEA-hydride spectra are normalized in intensity for ease of comparison.

peak. Thus, we interpret the high-energy shoulder as a feature originating from two-phonon scattering. An *in silico* INS spectra of TiH_2 calculated with two quantum events is given in the Supplementary information (Fig. S2).

Deuterides of TiVZrNbHf have in previous studies shown occupation of deuterium in both octahedral and tetrahedral sites [8,38,39]. Hydrogen occupying an octahedral position in a fcc lattice should also be observable as a separated peak in INS at lower energy transfers (60–80 meV for rare earths [17–19] and 60–120 for group VI-VIII transition metals [43]) than the peak corresponding to the tetrahedral position. To verify this we have also calculated the *in silico* spectra for NaCl-type metal monohydrides, which are presented in Fig. 3. These spectra show that peaks from hydrogen in octahedral environments would be in the energy transfer range 80–140 meV, i.e. at lower energy transfers than the tetrahedral sites. Of the monohydrides, HfH and ZrH would have the lowest and highest energy peaks respectively. Considering that, the

contributions of these individual metal monohydrides produces values that correlate well with the low energy transfer shoulder observed in the experimental INS spectra for the compositions $TiVZrNbH_x$, $TiVZrNbHf_{0.5}H_x$ and $TiVZrNbHfH_x$. We find this result indicative of interstitial hydrogen incorporated at octahedral sites in the structure for these compositions in agreement with references [8,38].

The optical peak energy of metal hydrides has been suggested to be directly relatable to the M-H distance [15,16,48]. Although the exact relationship is at a debate, it is clear that the longer the distance, the lower the vibrational peak energy, corresponding to a less tightly bonded state. The two main correlations found in the literature are a linear relationship proposed by Sakamoto (Sakamoto line) and an exponential relationship ($E(R) = AR^{-3/2}$) as proposed by Ross et al. (Ross correlation) which are shown as dashed-dotted and dashed lines respectively in Fig. 5 [15,48]. However, it has been shown that these correlation are mostly valid for di-hydrides since
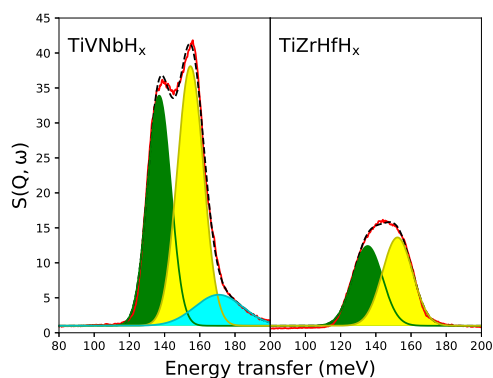
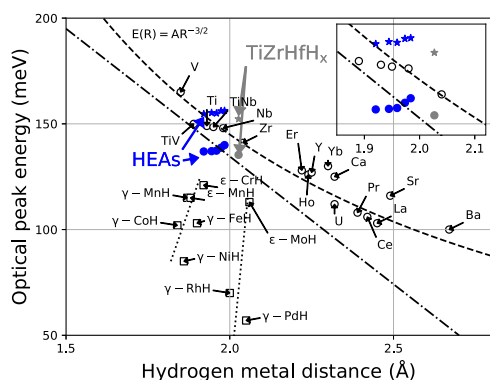**Fig. 4.** Gaussian fits to the experimental INS spectra of TiVNbH$_x$ (left) and TiZrHfH$_x$ (right).

Fig. 5. Correlation of optical peak energy against hydrogen to metal distance. The first and second HEA peaks are marked as circles and stars respectively. Literature values are taken from references [15,48]. The Sakamoto line and Ross correlation are shown as dashed-dotted and dashed lines respectively.

INS spectra of monohydrides of group VI-VIII transition metals synthesized at high pressures have shown an increase in peak energy with increasing metal-hydrogen distance [43]. This effect was attributed to an increase in the metal-hydrogen interactions caused by less efficient screening of core charges with decreasing number of valance electrons to the right in the periodic table.

To put the HEA-based metal hydrides in context with the INS literature on metal hydrides and to investigate the effect of having multiple closely related metal-hydrogen distances, the optical peak energies were extracted by deconvolution of the experimental HEA hydrides spectra. The INS spectra of TiZrHfH$_x$ can be fitted with two Gaussians (shown to the right in Fig. 4) with optical peaks at 139 and 152 meV respectively. This is close to the reported values of TiH$_2$ (149 meV) and ZrH$_2$ (141 meV) reported in reference [15]. On the other side, the INS spectra of TiVNbH$_x$ requires at least three Gaussians (137, 155 and 171 meV respectively) for a satisfactory fit. This is due to the high-energy shoulder discussed previously. Once Hf is added, a fourth Gaussian is required to account for the additional shoulder to the lower energy side.

Considering the extracted peak positions from the INS spectra of the HEA-based metal hydrides together with the M-H distance (average M-H distance in the case of HEAs) metal-H distance trend mentioned above yields the observations presented in Fig. 5. Firstly, we observe that the first optical peaks are centered on the Sakamoto line rather than the Ross correlation (similar to TiV), although some are rather close. Secondly, the second peak is close to and above the Ross line. This puts them closer to the behavior of some of the ionic metal hydrides such as CaH$_2$ or SrH$_2$. The trend among the HEAs is also the opposite of both the Sakamoto and Ross correlations (with the exception of TiZrHfH$_x$), where the peak energy of the HEAs are

seen to increase instead of decrease with longer M-H distances, putting them closer to the trend observed in the literature for group VI-VIII metal monohydrides [43].

This trend among the HEA-based metal hydrides suggests that they exhibit stronger metal-hydrogen interactions with increasing distances. If this is an effect of less screening by the valance electrons as was suggested in reference [43], it cannot be attributed to the valency alone since all the studied HEA are made of early transition metals. The steepening of the potential well must therefore originate of some other effect that this kind of alloying strategy has on the electronic structure. Reference [43] also showed a major difference between monohydrides of 3d and 4d transition metals where the peak energies of the 4d metal hydrides are lower in energy than what is expected from their much longer metal-hydrogen distances. This is similar to what is observed in the present work for TiZrHfH$_x$ where high concentrations of 4d and 5d metals are present while keeping *VEC* at 4.0. It is therefore evident that the full electronic structure of the alloy has to be taken into account when predicting the strength of metal-hydrogen interactions in HEAs, but *VEC* alone can give a good first indication as has been reported in the literature [7,39].

The peaks of the HEAs are generally very broad and it is therefore viable that they represent a distribution of different M-H distances as reported in [46]. In this case, the local environment themselves could fit better with the Ross correlation. No correlation could be found between the peak energies and the "HEA-parameters" atomic size-mismatch, *VEC* or electronegativity as can be seen in the Supplementary information (Fig. S4).

4. Conclusions

The present work has probed the vibrational properties of a series of HEA-based metal hydrides by inelastic neutron scattering. The main feature of the spectra is the optical peak centered around 150 meV of hydrogen vibrating within a tetrahedral interstitial site in a CaF$_2$-type structure. TiVNbH$_x$ showed a split in this peak similar to what has been observed for ZrH$_2$. This feature becomes less pronounced as more elements are added, which is most likely due to the peaks broadening with additional M-H distances present. The splitting of the optical peak is identified by DFT to originate from different phonons and not structural distortions. *In silico* INS spectra of binary transition metal hydrides indicate that the higher energy shoulder observed in all investigated compositions originates from two-phonon neutron scattering, and the lower energy shoulders from H occupation in octahedral interstitials. Correlations between the peak energy and the metal-hydrogen distance indicated that not only the valance electron concentration plays a role in determining the strength of the M-H bond in HEAs.

CRediT authorship contribution statement

Gustav Ek: Conceptualization, Formal analysis, Investigation, Visualization, Writing - original draft, Writing - review & editing. **Øystein S. Fjellvåg:** Formal analysis, Writing - original draft, Writing - review & editing. **Ponniah Vajeseton:** Software, Writing - original draft. **Jeff Armstrong:** Investigation, Writing - review & editing. **Martin Sahlberg:** Supervision. **Ulrich Häussermann:** Supervision, writing - review & editing.

Declaration of Competing Interest

The authors declare that they have no known competing financial interests or personal relationships that could have appeared to influence the work reported in this paper.

Acknowledgements

Appendix A. Supporting information

Supplementary data associated with this article can be found in the online version at doi:10.1016/j.jallcom.2021.160320.

References

[1] B. Cantor, I.T.H. Chang, P. Knight, A.J.B. Vincent, Microstructural development in equiatomic multicomponent alloys, Mater. Sci. Eng. A 375–377 (2004) 213–218, https://doi.org/10.1016/j.msea.2003.10.257

[2] Y.F. Ye, Q. Wang, J. Lu, C.T. Liu, Y. Yang, High-entropy alloy: challenges and prospects, Mater. Today 19 (6) (2016) 349–362, https://doi.org/10.1016/j.mattod.2015.11.026

[3] I. Kunce, M. Polanski, J. Bystrzycki, Microstructure and hydrogen storage properties of a TiZrNbMoV high entropy alloy synthesized using Laser Engineered Net Shaping (LENS), Int. J. Hydrog. Energy 39 (18) (2014) 9904–9910, https://doi.org/10.1016/j.ijhydene.2014.02.067

[4] I. Kunce, M. Polanski, J. Bystrzycki, Structure and hydrogen storage properties of a high entropy ZrTiVCrFeNi alloy synthesized using Laser Engineered Net Shaping (LENS), Int. J. Hydrog. Energy 38 (27) (2013) 12180–12189, https://doi.org/10.1016/j.ijhydene.2013.05.071

[5] M. Sahlberg, D. Karlsson, C. Zlotea, U. Jansson, Superior hydrogen storage in high entropy alloys, Sci. Rep. 6 (2016) 1–6, https://doi.org/10.1038/srep36770

[6] M.M. Nygård, G. Ek, D. Karlsson, M. Sahlberg, M.H. Sørby, B.C. Hauback, Hydrogen storage in high-entropy alloys with varying degree of local lattice strain, Int. J. Hydrog. Energy 44 (55) (2019) 29140–29149, https://doi.org/10.1016/j.ijhydene.2019.03.223

[7] M.M. Nygård, G. Ek, D. Karlsson, M.H. Sørby, M. Sahlberg, B.C. Hauback, Counting electrons - A new approach to tailor the hydrogen sorption properties of high-entropy alloys, Acta Mater. 175 (2019) 121–129, https://doi.org/10.1016/j.actamat.2019.06.002

[8] D. Karlsson, G. Ek, J. Cedervall, C. Zlotea, K.T. Møller, T.C. Hansen, J. Bednarčík, M. Paskevicius, M.H. Sørby, T.R. Jensen, U. Jansson, M. Sahlberg, Structure and hydrogenation properties of a HfNbTiVZr high-entropy alloy, Inorg. Chem. 57 (4) (2018) 2103–2110, https://doi.org/10.1021/acs.inorgchem.7b03004

[9] C. Zlotea, M.A. Sow, G. Ek, J.P. Couzinié, L. Perrière, I. Guillot, J. Bourgon, K.T. Møller, T.R. Jensen, E. Akiba, M. Sahlberg, Hydrogen sorption in TiZrNbHfTa high entropy alloy, J. Alloy. Compd. 775 (2019) 667–674, https://doi.org/10.1016/J.JALLCOM.2018.10.108

[10] C. Zhang, Y. Wu, L. You, X. Cao, Z. Lu, X. Song, Investigation on the activation mechanism of hydrogen absorption in TiZrNbTa high entropy alloy, J. Alloy. Compd. 781 (2019) 613–620, https://doi.org/10.1016/j.jallcom.2018.12.120

[11] H. Shen, J. Zhang, J. Hu, J. Zhang, Y. Mao, H. Xiao, X. Zhou, X. Zu, A novel TiZrHfMoNb high-entropy alloy for solar thermal energy storage, Nanomaterials 9 (2) (2019) 248, https://doi.org/10.3390/nano9020248

[12] J. Montero, C. Zlotea, G. Ek, J.-C. Crivello, L. Laversenne, M. Sahlberg, TiVZrNb Multi-Principal-Element Alloy: Synthesis Optimization, Structural, and Hydrogen Sorption Properties, Molecules 24 (15) (2019) 2799, https://doi.org/10.3390/molecules24152799

[13] J. Hauck, H.J. Schenk, The coordination of hydrogen in transition metal hydrides, J. Less Common Met. 51 (2) (1977) 251–258, https://doi.org/10.1016/0022-5088(77)90086-8

[14] X. Xin, R. Johansson, M. Wolff, B. Hjörvarsson, Hydrogen in vanadium: Site occupancy and isotope effects, Phys. Rev. B 93 (13) (2016) 1–5, https://doi.org/10.1103/PhysRevB.93.134107

[15] D.K. Ross, P.F. Martin, W.A. Oates, R.K. Bakhsh, Inelastic neutron scattering measurements of optical vibration frequency distributions in hydrogen-metal systems, Z. für Phys. Chem. 114 (114) (1979) 221–230, https://doi.org/10.1524/zpch.1979.114.114.221

[16] Y. Fukai, H. Sugimoto, On the optical-mode excitation energy interstitial hydrogen in metals, J. Phys. F Met. Phys. 11 (7) (1981) L137–L139, https://doi.org/10.1088/0305-4608/11/7/001

[17] T.J. Udovic, J.J. Rush, I.S. Anderson, Neutron spectroscopic comparison of β-phase rare earth hydrides, J. Alloy. Compd. 231 (1–2) (1995) 138–143, https://doi.org/10.1016/0925-8388(95)01788-7

[18] T.J. Udovic, J.J. Rush, I.S. Anderson, Characterization of the vibrational dynamics in the octahedral sublattices of LaD 2.25 and LaH 2.25, J. Phys. Condens. Matter 7 (35) (1995) 7005–7014, https://doi.org/10.1088/0953-8984/7/35/007

[19] T.J. Udovic, J.J. Rush, I.S. Anderson, Neutron spectroscopic evidence of concentration-dependent hydrogen ordering in the octahedral sublattice of β-TbH2+x, Phys. Rev. B 50 (10) (. 1994) 7144–7146, https://doi.org/10.1103/PhysRevB.50.7144

[20] S.K. Callear, A.J. Ramirez-Cuesta, K. Kamazawa, S. Towata, T. Noritake, S.F. Parker, M.O. Jones, J. Sugiyama, M. Ishikiriyama, W.I. David, Understanding composition-property relationships in Ti-Cr-V-Mo alloys for optimisation of hydrogen storage in pressurised tanks, Phys. Chem. Chem. Phys. 16 (31) (2014) 16563–16572, https://doi.org/10.1039/C4CP01666A

[21] J.G. Couch, O.K. Harling, L.C. Clune, Structure in the Neutron Scattering Spectra of Zirconium Hydride, Phys. Rev. B 4 (8) (1971) 2675–2681, https://doi.org/10.1103/PhysRevB.4.2675

[22] H.W. Brinks, A. Fossdal, R.C. Bowman, B.C. Hauback, Pressure–composition isotherms of TbNiAlHx, J. Alloy. Compd. 417 (1–2) (2006) 92–95, https://doi.org/10.1016/j.jallcom.2005.09.018

[23] H.M. Rietveld, A profile refinement method for nuclear and magnetic structures, J. Appl. Crystallogr. 2 (2) (1969) 65–71, https://doi.org/10.1107/S0021889869006558

[24] A.A. Coelho, TOPAS and TOPAS-Academic: an optimization program integrating computer algebra and crystallographic objects written in C++, J. Appl. Crystallogr. 51 (1) (2018) 210–218, https://doi.org/10.1107/S1600576718000183

[25] R.S. Pinna, S. Rudić, S.F. Parker, J. Armstrong, M. Zanetti, G. Škoro, S.P. Waller, D. Zacek, C.A. Smith, M.J. Capstick, D.J. McPhail, D.E. Pooley, G.D. Howells, G. Gorini, F. Fernandez-Alonso, The neutron guide upgrade of the TOSCA spectrometer, Nucl. Instrum. Methods Phys. Res. Sect. A Accel. Spectrom. Detect. Assoc. Equip. 896 (2018) 68–74, https://doi.org/10.1016/j.nima.2018.04.009

[26] G. Ek, M. Sahlberg, U. Häussermann, Vibrational property study of high entropy alloy (HEA) hydrides, STFC ISIS Neutron Muon Source (2019), https://doi.org/10.5286/ISIS.E.101134198

[27] G. Kresse, J. Furthmüller, Efficient iterative schemes for ab initio total-energy calculations using a plane-wave basis set, Phys. Rev. B 54 (16) (1996) 11169–11186, https://doi.org/10.1103/PhysRevB.54.11169

[28] G. Kresse, J. Furthmüller, Efficiency of ab-initio total energy calculations for metals and semiconductors using a plane-wave basis set, Comput. Mater. Sci. 6 (1) (1996) 15–50, https://doi.org/10.1016/0927-0256(96)00008-0

[29] J.P. Perdew, K. Burke, M. Ernzerhof, Generalized gradient approximation made simple, Phys. Rev. Lett. 77 (18) (1996) 3865–3868, https://doi.org/10.1103/PhysRevLett.77.3865

[30] A.I. Liechtenstein, V.I. Anisimov, J. Zaanen, Density-functional theory and strong interactions: orbital ordering in Mott-Hubbard insulators, Phys. Rev. B 52 (8) (1995) R5467–R5470, https://doi.org/10.1103/PhysRevB.52.R5467

[31] S.L. Dudarev, G.A. Botton, S.Y. Savrasov, Z. Szotek, W.M. Temmerman, A.P. Sutton, Electronic structure and elastic properties of strongly correlated metal oxides from first principles: LSDA + U, SIC-LSDA and EELS Study of UO2 and NiO, Phys. Status Solidi 166 (1) (1998) 429–443 doi: 10.1002/(SICI)1521-396X(199803)166:1 < 429::AID-PSSA429 > 3.0.CO;2-F.

[32] A. Togo, F. Oba, I. Tanaka, First-principles calculations of the ferroelastic transition between rutile-type andCaCl2-typeSiO2at high pressures, Phys. Rev. B 78 (13) (2008) 134106, https://doi.org/10.1103/PhysRevB.78.134106

[33] H.J. Monkhorst, J.D. Pack, Special points for Brillouin-zone integrations, Phys. Rev. B 13 (12) (1976) 5188–5192, https://doi.org/10.1103/PhysRevB.13.5188

[34] J. Armstrong, A.J. O'Malley, M.R. Ryder, K.T. Butler, Understanding dynamic properties of materials using neutron spectroscopy and atomistic simulation, J. Phys. Commun. 4 (7) (2020) 072001, https://doi.org/10.1088/2399-6528/ab9c2e

[35] O. Arnold, J.C. Bilheux, J.M. Borreguero, A. Buts, S.I. Campbell, L. Chapon, M. Doucet, N. Draper, R. Ferraz Leal, M.A. Gigg, V.E. Lynch, A. Markvardsen, D.J. Mikkelson, R.L. Mikkelson, R. Miller, K. Palmen, P. Parker, G. Passos, T.G. Perring, P.F. Peterson, S. Ren, M.A. Reuter, A.T. Savici, J.W. Taylor, R.J. Taylor, R. Tolchenov, W. Zhou, J. Zikovsky, Mantid—Data analysis and visualization package for neutron scattering and μSR experiments, Nucl. Instrum. Methods Phys. Res. Sect. A Accel. Spectrometers, Detect. Assoc. Equip. 764 (2014) 156–166, https://doi.org/10.1016/j.nima.2014.07.029

[36] K. Dymkowski, S.F. Parker, F. Fernandez-Alonso, S. Mukhopadhyay, AbINS: the modern software for INS interpretation, Phys. B Condens. Matter 551 (2018) 443–448, https://doi.org/10.1016/j.physb.2018.02.034

[37] D. Karlsson, G. Ek, J. Cedervall, C. Zlotea, K.T. Møller, T.C. Hansen, J. Bednarčík, M. Paskevicius, M.H. Sørby, T.R. Jensen, U. Jansson, M. Sahlberg, Structure and hydrogenation properties of a HfNbTiVZr high-entropy alloy, Inorg. Chem. 57 (4) (2018) 2103–2110, https://doi.org/10.1021/acs.inorgchem.7b03004

[38] M.M. Nygård, W.A. Sławiński, G. Ek, M.H. Sørby, M. Sahlberg, D.A. Keen, B.C. Hauback, Local order in high-entropy alloys and associated deuterides – a total scattering and Reverse Monte Carlo study, Acta Mater. 199 (2020) 504–513, https://doi.org/10.1016/j.actamat.2020.08.045

[39] G. Ek, M.M. Nygård, A.F. Pavan, J. Montero, P.F. Henry, M.H. Sørby, M. Witman, V. Stavila, C. Zlotea, B.C. Hauback, M. Sahlberg, Elucidating the effects of the composition on hydrogen sorption in tivzrnbhf-based high-entropy alloys, Inorg. Chem. 60 (2) (2021) 1124–1132, https://doi.org/10.1021/acs.inorgchem.0c03270

[40] V. Pacheco, G. Lindwall, D. Karlsson, J. Cedervall, S. Fritze, G. Ek, P. Berastegui, M. Sahlberg, U. Jansson, Thermal stability of the HfNbTiVZr high-entropy alloy, Inorg. Chem. 58 (1) (2019) 811–820, https://doi.org/10.1021/acs.inorgchem.8b02957

[41] R. Hempelmann, D. Richter, O. Hartmann, E. Karlsson, R. Wäppling, The positive muon in the intermetallic hydride ZrV 2H x: A muon tracer study supplemented by differential thermoanalysis, neutron vibrational spectroscopy, and quasielastic neutron scattering, J. Chem. Phys. 90 (3) (1989) 1935–1949, https://doi.org/10.1063/1.456672

[42] T. Ueda, S. Hayashi, Y. Nakai, S. Ikeda, Local structure in ß-Ti1-yVyHx studied by inelastic neutron scattering, Phys. Rev. B 51 (9) (1995) 5725–5731, https://doi.org/10.1103/PhysRevB.51.5725

[43] A.I. Kolesnikov, V.E. Antonov, V.K. Fedotov, G. Grosse, A.S. Ivanov, F.E. Wagner, Lattice dynamics of high-pressure hydrides of the group VI–VIII transition metals, Phys. B Condens. Matter 316–317 (2002) 158–161, https://doi.org/10.1016/S0921-4526(02)00447-7

[44] D. Chattaraj, S.C. Parida, S. Dash, C. Majumder, First principles study of the ZrX2 (X = H, D and T) compounds, Int. J. Hydrog. Energy 39 (18) (2014) 9681–9689, https://doi.org/10.1016/j.ijhydene.2014.04.094

[45] J. Blomqvist J. Olofsson A.-M. Alvarez C. Bjerkén. Structure and Thermodynamical Properties of Zirconium Hydrides, in: Proceedings of the 15th International Conference on Environmental Degradation of Materials in Nuclear Power Systems — Water Reactors 2011 pp. 671-681.

[46] M.M. Nygård, Ø.S. Fjellvåg, M.H. Sørby, K. Sakaki, K. Ikeda, J. Armstrong, P. Vajeeston, W.A. Sławiński, H. Kim, A. Machida, Y. Nakamura, B.C. Hauback, The average and local structure of TiVCrNbDx(x=0,2.2,8) from total scattering and neutron spectroscopy, Acta Mater. 205 (2021) 116496, https://doi.org/10.1016/j.actamat.2020.116496

[47] T.J. Udovic, J.J. Rush, I.S. Anderson, R.G. Barnes, Hydrogen vibrational modes and anisotropic potential in α - ScH x, Phys. Rev. B 41 (6) (1990) 3460–3465, https://doi.org/10.1103/PhysRevB.41.3460

[48] M. Sakamoto, Studies of hydrogen vibrations in transition metal hydrides by thermal neutron transmissions, J. Phys. Soc. Jpn. 19 (10) (1964) 1862–1866, https://doi.org/10.1143/JPSJ.19.1862